### Title
Toward real-time, volumetric dosimetry for FLASH-capable clinical synchrocyclotrons using protoacoustic imaging




### Journal
Medical Physics, 51(11)

### ISSN
0094-2405



### Authors
Wang, Siqi
Gonzalez, Gilberto
Owen, Daniel Rocky
et al.



### Publication Date
2024-11-01

### DOI
10.1002/mp.17318

Peer reviewed

HHS Public Access

Author manuscript

*Med Phys*. Author manuscript; available in PMC 2024 November 02.

Published in final edited form as:

*Med Phys*. 2024 November ; 51(11): 8496–8505. doi:10.1002/mp.17318.

# Toward real-time, volumetric dosimetry for FLASH-capable clinical synchrocyclotrons using protoacoustic imaging

**Siqi Wang**[1], **Gilberto Gonzalez**[2], **Daniel Rocky Owen**[3], **Leshan Sun**[1], **Yan Liu**[3], **Townsend Zwart**[3], **Yong Chen**[2], **Liangzhong Xiang**[1,4,5]

[1]The Department of Biomedical Engineering, University of California, Irvine, California, USA

[2]Department of Radiation Oncology, University of Oklahoma Health Sciences Center, Oklahoma City, Oklahoma, USA

[3]Mevion Medical Systems, Littleton, Massachusetts, USA

[4]Beckman Laser Institute & Medical Clinic, University of California, Irvine, California, USA

[5]Department of Radiological Sciences, University of California, Irvine, California, USA

## Abstract

**Background:** Fast low angle shot hyperfractionation (FLASH) radiotherapy (RT) holds promise for improving treatment outcomes and reducing side effects but poses challenges in radiation delivery accuracy due to its ultra-high dose rates. This necessitates the development of novel imaging and verification technologies tailored to these conditions.

**Purpose:** Our study explores the effectiveness of proton-induced acoustic imaging (PAI) in tracking the Bragg peak in three dimensions and in real time during FLASH proton irradiations, offering a method for volumetric beam imaging at both conventional and FLASH dose rates.

**Methods:** We developed a three-dimensional (3D) PAI technique using a 256-element ultrasound detector array for FLASH dose rate proton beams. In the study, we tested protoacoustic signal with a beamline of a FLASH-capable synchrocyclotron, setting the distal 90% of the Bragg peak around 35 mm away from the ultrasound array. This configuration allowed us to assess various total proton radiation doses, maintaining a consistent beam output of 21 pC/pulse. We also explored a spectrum of dose rates, from 15 Gy/s up to a FLASH rate of 48 Gy/s, by administering a set number of pulses. Furthermore, we implemented a three-dot scanning beam approach to observe the distinct movements of individual Bragg peaks using PAI. All these procedures utilized a proton beam energy of 180 MeV to achieve the maximum possible dose rate.

**Results:** Our findings indicate a strong linear relationship between protoacoustic signal amplitudes and delivered doses $\left(R^2 = 0.9997\right)$, with a consistent fit across different dose rates.

**Correspondence**: Liangzhong Xiang, The Department of Biomedical Engineering, University of California, Medical Sciences, B-134, Irvine, CA 92697–5000, USA. liangzhx@hs.uci.edu.
Siqi Wang and Gilberto Gonzalez contributed equally to this study.

CONFLICT OF INTEREST STATEMENT
The authors declare no conflicts of interest.

SUPPORTING INFORMATION
Additional supporting information can be found online in the Supporting Information section at the end of this article.

The technique successfully provided 3D renderings of Bragg peaks at FLASH rates, validated through absolute Gamma index values.

**Conclusions:** The protoacoustic system demonstrates effectiveness in 3D visualization and tracking of the Bragg peak during FLASH proton therapy, representing a notable advancement in proton therapy quality assurance. This method promises enhancements in protoacoustic image guidance and real-time dosimetry, paving the way for more accurate and effective treatments in ultra-high dose rate therapy environments.

**Keywords**

FLASH proton; in vivo dosimetry; protoacoustics

## 1 | INTRODUCTION

Proton beam therapy is distinguished by its unique Bragg peak depth-dose curves, which allow for precise dose deposition at specific tissue depths. This characteristic is particularly beneficial compared to photon-based therapies, which can affect tissues both in front and beyond the target tumor.[1] Proton therapy is especially advantageous when treating areas close to sensitive organs or in pediatric cases, where minimizing treatment toxicity is crucial.[2–4] The focused energy delivery of the Bragg peak ensures minimal damage to surrounding healthy tissue, making proton therapy superior in terms of precision and safety.[5–8]

Typically, proton therapy involves administering doses of 60–80 Gy over several weeks through daily sessions, a process known as conventional fractionation.[9] However, the field has seen a burgeoning interest in the biological effects of ultra-high dose rate or Fast Low Angle Shot Hyperfractionation(FLASH) therapy, which delivers high doses at rates exceeding conventional methods.[10–12] FLASH therapy (> 40 Gy/s) has shown promise in animal studies for its ability to preserve healthy tissue while effectively controlling tumor growth, with notable outcomes such as the memory-sparing effect in mice.[13–17]

Despite the potential of FLASH therapy, challenges remain, including identifying optimal beam conditions and understanding the biological mechanisms involved. Clinical synchrocyclotrons, capable of accelerating protons and modulating their range and direction, enable the application of intensity-modulated proton therapy (IMPT) and are exploring hypofractionation or single-fraction treatments in the context of FLASH therapy.[18,19]

The precision of proton therapy, however, is dependent on the accurate placement of the Bragg peak, necessitating real-time in vivo imaging to ensure the correct dose delivery while protecting surrounding healthy tissues.[20] This is particularly critical in FLASH irradiation, where rapid dose changes and unique beam properties demand advanced monitoring techniques. Traditional quality assurance methods fall short in this high-dose-rate context,[21,22] prompting a shift toward real-time imaging for both temporal and spatial dose distribution and the development of faster, more adaptive detectors.[16,23–25]

Among the emerging technologies, Proton-induced Acoustic Imaging (PAI) shows promise for localizing the Bragg peak and providing real-time in vivo dosimetry.[26–32] PAI employs acoustic waves generated by the energy deposition from proton beams in tissues to determine the delivered radiation dose, exploiting the Bragg peak phenomenon to precisely map out dose distributions.[33,34] Despite the potential of PAI, previous studies have not demonstrated that PAI is capable of reconstructing the FLASH rate proton beam Bragg peak in water in three dimensions (3D).

In this paper, we introduce a strategy that employs PAI for high-precision range verification in 3D and real-time dose monitoring during proton therapy. The ability of the protoacoustic imaging system to measure proton dose rates from clinical to FLASH rates, and its capacity for 3D visualization of the Bragg peak, highlight the potential of PAI in enhancing real-time adaptive radiotherapy. The linearity of the PAI dosimeter has been validated, and the technique's capacity to track individual Bragg peak movements during pencil beam scanning underscores its value for future applications in real-time adaptive radiotherapy.

## 2 | MATERIALS AND METHODS

### 2.1 | Theory of protoacoustics

The fundamental concepts of protoacoustics are grounded in the thermoacoustic effect, which suggests that when a target is irradiated by an energy source, it emits pressure waves. Specifically, when a proton beam targets an object, the most prominent pulse emission occurs at the Bragg peak. The behavior of these protoacoustic waves is governed by the wave equation[35,36]:

$$\nabla^2 p(\vec{r},t) - \frac{1}{v_s^2}\frac{\partial^2}{\partial t^2}p(\vec{r},t) = -\frac{\beta}{C_p}\frac{\partial}{\partial t}H(\vec{r},t) \tag{1}$$

In this equation, $H(\vec{r},t)$ refers to the heat deposition at point $\vec{r}$ and time $t$, $v_s$ denotes the speed of sound in the medium, $\beta$ signifies the thermal expansion coefficient, and $C_p$ represents the specific heat capacity. The complexity of this pressure wave equation can be reduced by assuming that each individual proton pulse deposits energy instantaneously. The resolution to Equation (1) due to pulse excitation is as follows [37]:

$$P_0(\vec{r},t) = \frac{\beta}{4\pi C_p}\frac{\partial}{\partial t}\left(\frac{1}{ct}\int_{S(\vec{r},t)} H(\vec{r}')dS'(t)\right); \left|\vec{r}-\vec{r}'\right| = ct \tag{2}$$

In this case, $S'(t)$ signifies a time-variable spherical surface at the detector's central location $(\vec{r})$ such that $\left|\vec{r}-\vec{r}'\right| = ct$ . $P_0(\vec{r},t)$ represents the initial pressure rise at the location $(\vec{r})$ and at time $t$. Through time-of-flight information from proton-induced acoustic pulses, the precise location of the Bragg peak can be determined. Ultrasound transducers attached to the patient capture the 3D acoustic waves, enabling the reconstruction of 2D and 3D images from PAI signals and thus allowing for real-time mapping of dose deposition.

The relationship between each proton pulse's dose and the resultant acoustic pressure is given by:

$$P_0 = \Gamma \rho D \tag{3}$$

Here, Γ stands for the Gruneisen coefficient, a dimensionless parameter, and $\rho$ signifies the material density. This equation crucially links the measured protoacoustic amplitude $P$ with the deposited radiation dose $D$, facilitating direct dose measurement for each individual pulse.[26,38,39] Previous research has established the linearity between dose and acoustic signal at conventional rates, which recent studies have extended to FLASH dose rates using electron beams, and even to higher instantaneous rates with laser-driven accelerators.[40,41]

## 2.2 | 3D image reconstruction

We implemented a wavelet denoising algorithm in our research,[42] enabling the detection of individual FLASH proton pulses. This method was instrumental in improving data clarity, serving as a crucial step toward successful image reconstruction for a single FLASH proton pulse. To further boost the signal-to-noise ratio (SNR), we employed a technique of averaging and consolidating data from up to 2000 frames to refine the quality of our reconstructions. Our PAI imaging setup featured a 256-element matrix array, measuring 4.8 cm by 4.8 cm. The reconstruction was performed on a grid that matched the array's lateral dimensions with a voxel resolution of 400 $\mu m^3$. For the 3D image reconstruction, we utilized the Universal Back-Projection (UBP) algorithm,[42] renowned for its efficacy in reconstructing 3D acoustic images in various research contexts. This strategic approach allowed us to accurately reconstruct dose maps and localize the Bragg peak.

## 2.3 | Experimental setup

Figure 1a describes the overall experimental setup for the study. This study utilized a synchrocyclotron proton therapy system (HYPERSCAN, Mevion Medical Systems, Littleton, USA) (Figure 1b) that employs a compact 8 Tesla superconducting synchrocyclotron to accelerate protons to 230 MeV (range approximately 32 $g/cm^2$).[43] Furthermore, the Mevion FLASH Research Kit was used to facilitate and control FLASH deliveries. To boost the current and produce remarkably high FLASH dose rates, several system parameters were meticulously adjusted. These modifications included setting an emission voltage of −1.5 kV on the ion source cathodes and determining a signal amplitude based on empirical data, usually around ~10 kV. A crucial step was the precise alignment of the superconducting coil with the warm accelerator iron, maintaining a tolerance of less than 0.5 mm. A pulse repetition frequency of $f = 756$ Hz was utilized in this study. The output dose rate was controlled through pulse width modulation of the ion source, with durations varying from 12.5 to 26 μs. Table 1 describes the key parameters of the proton beam used for experiments and reference dose measurements. Only the dose rate versus protoacoustic amplitude comparison experiments used different ion source pulse width from 8 to 14 μs. All other tests used the maximum 14 μs of the ion source pulse width. The reference measurements were performed with a PPC05 (IBA Dosimetry GmbH, Germany)

and FLASH-capable transmission (FLASH TIC) ion chamber using the same measurement configurations described in a previous study for the same machine.[43]

As shown in Figure 1a, a custom matrix-array detector (Doppler Electronic Technologies Co., Ltd., Guangzhou, China) was employed for PAI wave collection. The ultrasound detector has a center frequency of 1 MHz and 60% bandwidth. During the experiment, the detector was submerged in a water tank and lifted to the proton beam height. For all tests done in this study, the planar array detector was placed 33.2 cm away from the calculated Bragg peak depth. For accurate acquisition timing, a plastic scintillator at the beam height was used for synchronization between the proton beam firing and the acoustic wave collection. All data collection was carried out using a 256-channel data acquisition system (Legion ADC, Photosound Technology, Houston, USA), which had been previously tailored to include an extra 49 dB preamplification stage prior to the analog-digital conversion.

To showcase the 3D imaging capabilities of our PAI system in identifying the Bragg peak within the FLASH domain, we administered a FLASH proton beam in a water tank. The ion source's pulse width was set at 14 μs, delivering an estimated total dose of 544 Gy over 13.2 s, equating to a dose rate of 41 Gy/s in the FLASH region. For improved 3D image quality,1000 out of 5000 pulses were processed and averaged for the final Bragg peak 3D reconstruction. In addition to 3D volumetric display of the Bragg peak, or dosimetric validation, a Gafchromic EBT3 radiochromic film was used, irradiated at the same depth as the PAI Bragg peak, providing a benchmark for dosimetry performance.

In studying the use of ultra-high dose rate radiotherapy, also known as "FLASH" therapy, it is crucial to measure the total dose and dose rate accurately due to the shorter timescales involved compared to conventional radiation. The dose rate (Gy/s), indicates the amount of dose deposited in the tissue each second, depending on the dose per pulse and the repetition rate of the system. Our investigation assessed five different total dose levels:50, 75, 100, 200, and 300 Gy, using PAI measurements. These levels were tested three times each to ensure statistical accuracy. During these tests, we maintained a consistent dose rate of approximately 48 Gy/s, with a fixed charge of 21 pC/pulse. While keeping constant dose rate, we varied the number of pulses to align with the total desired dose. The total dose measurements compiled were essentially the cumulative sum of all acquired acoustic amplitudes, correlating to the total dose administered. Furthermore, to validate the effectiveness of the PAI system in measuring the total proton beam dose rate within the FLASH range, we conducted tests on a prototype proton beam, adjusting the total dose rate outputs from a standard clinical dose rate of 15.2 Gy/s up to a FLASH dose rate of 48 Gy/s. By modifying the dose rate output while maintaining a pulse repetition frequency of 750 Hz, we were able to extract acoustic amplitudes from varying output intensities. Each dose rate level was tested five times, and every measurement represented an average of 1000 proton pulses to minimize background noise interference.

The PAI system represents a new approach for real-time tracking of proton pencil beam scanning during FLASH Radiotherapy (RT) delivery. This technology enables three-dimensional (3D) volumetric dosimetric reconstruction for a single proton pulse, enhancing the accuracy and effectiveness of radiotherapy. In an application of this system, the PAI

monitored the movements of a proton beam adjusted to three different positions, each set 5 mm apart. The monitoring was facilitated by a planar array detector positioned 33.2 cm from the plane of Bragg peak movements, which remained stationary during data collection. The analysis led to the generation of visual representations, accurately tracing the movement of Bragg peaks during pencil beam scanning.

## 3 | RESULTS

### 3.1 | Volumetric image of the Bragg peak

Figures 2a, 2b show the protoacoustic imaging for lateral and axial reconstructions, respectively, with profile lines indicating the center of each slice. The dashed white lines illustrate the profile lines' origins, demonstrating accurate Bragg peak reconstruction at a 42 Gy/s dose rate. The lateral profile (yellow line) forms a Gaussian distribution with a 21 mm full width at half maximum (FWHM), while the red curve in Figure 2b shows the axial profile with a 10 mm thickness from the 3D reconstructed Bragg peak.

The outcomes of the dosimetric validation test are shown in Figure 3,including the original (Figure 3a) and digitized film (Figure 3b) alongside the reconstructed PAI peak, with contour lines drawn at 60%, 80%, and 90% normalized dose intensity to compare shapes. The PAI peak appears more rounded, likely due to limited-view effects and large ultrasound element sizes. Absolute gamma index analysis, depicted in Figures 3d–f, demonstrates good alignment between PAI measurements and film in the peak's central area, with expected variations elsewhere due to back-projection algorithm limitations. Table 2 indicates that while the PAI method's accuracy is low for doses below 10% of the peak, it is accurate when presenting above 50% intensity across all standards, with areas above 30% intensity satisfactorily meeting the 5 mm/5% gamma index criteria, affirming the PAI method's effectiveness in accurate dose mapping.

### 3.2 | Dose linearity study in FLASH regime

The results demonstrated clear dose linearity in the FLASH region. Specifically, PAI signals from the proton beam, under different total dose levels, showed that the normalized amplitudes of acoustic signals linearly correlated with the actual administered doses, achieving a near-perfect $R^2$ value of 0.9997 (Figure 4a). This indicates a highly accurate representation of dose linearity at various levels. Additionally, the relationship between the measured dose rate delivered and the PAI acoustic amplitude followed a similar linear trend, with an $R^2$ value of 0.9782, validating the PAI system's ability to measure dose rates accurately within the FLASH region (Figure 4b). These findings confirm the dose linearity in the FLASH region, crucial for advancing precision in radiotherapy treatments. Figure 4c displays the averaged protoacoustic signals obtained from proton beams with dose rates of 15 and 48 Gy/s. Meanwhile, Figure 4d illustrates the typical frequency components of the acquired protoacoustic signals, using the signal from the 48 Gy/s proton beam as an example.

### 3.3 | Real-time tracking proton pencil beam scanning during FLASH RT delivery

The locations of the scanned Bragg peak are individually represented as reconstructed lateral slices in Figures 5a–c. Figure 5d presents a superimposed image where the movements of the Bragg peak are clearly outlined. Finally, the reconstructed dose distribution from three different locations was analyzed against the film results of the accumulated dose using the absolute gamma index. The subsequent passing region mapping is shown in Figure 5f, and the corresponding gamma index values are listed in Table 2. This experiment serves to illustrate the precision and real-time capabilities of PAI in tracking proton pencil beam scanning during FLASH RT delivery. The complete sequence of recorded proton Bragg peak movements can be seen in the supplementary Video S-1.

## 4 | DISCUSSIONS

PAI is emerging as a dosimetric tool for real-time monitoring of FLASH proton therapy, a form of radiotherapy that delivers ultra-high dose rate at a very short period of time. Our experiments confirm that PAI can maintain linearity within the FLASH regime, meaning it does not reach saturation even at high dose rates (48 Gy/s, shown in Figure 4b), which is crucial for accurate dose measurement and ensures real-time tracking capabilities. Adjustments can be made to the hardware to address any potential signal saturation, such as reducing the amplifier gain, have been shown to be effective. This suggests that with appropriate hardware modifications, PAI could monitor even higher doses per pulse without experiencing saturation, enhancing its applicability in FLASH RT.

While previous studies have demonstrated the potential of radiation-induced acoustic imaging for point measurement[44] and two-dimensional monitoring during proton therapy,[30,45,46] our study extends this by offering real-time, 3D monitoring at the single-pulse level. This research represents the first attempt where PAI has been used to create 3D volumetric dose maps specifically for FLASH therapy (Figure 2). These findings are vital because they indicate that PAI can be used to monitor and adjust treatment in real time, enhancing the safety and efficacy of FLASH proton therapy.

Nonetheless, challenges remain, such as the partial detection geometry and sparse elements in the transducer array, leading to certain artifacts in the reconstructed dose maps (Figure 2b). These issues highlight the need for further advancements in image reconstruction algorithms, such as model-based image reconstruction algorithm[47,48] and deep learning-based image reconstruction algorithm[27,49,50] which could mitigate problems like limited view and streak artifacts. Moreover, the resolution of PAI could be improved. The current study used a 1 MHz transducer array, balancing between detection sensitivity and spatial resolution constraints. Future developments could explore transducer arrays with higher sensitivity and finer element geometry, improving spatial resolution. Furthermore, using a narrow pulse duration of the proton beam that satisfies the stress confinement would potentially improve the high-frequency components of protoacoustic signals, thus, to improve the imaging resolution.

Moreover, integrating PAI with other imaging modalities, such as Computed Tomography (CT) scans, could further enhance dose deposition mapping and treatment accuracy. This

integration would leverage the detailed anatomical information from CT imaging, potentially leading to more precise and effective radiotherapy treatments.

## 5 | CONCLUSIONS

In conclusion, our study highlighted the effectiveness of PAI for real-time, 3D imaging of Bragg peak in the context of FLASH proton therapy. We successfully illustrated PAI's capacity to render Bragg peaks in three dimensions and to track lateral pencil beam scanning accurately. Notably, PAI distinguishes itself from conventional methodologies by its ability to consistently measure dose rates from standard clinical levels up to FLASH levels, thereby effectively monitoring each Bragg peak within FLASH beamlets. This development fills a crucial void in proton therapy, presenting opportunities for enhanced image guidance, precise in vivo dosimetry, and the provision of real-time, 3D dosimetric feedback.

## Supplementary Material

Refer to Web version on PubMed Central for supplementary material.

## ACKNOWLEDGMENTS

Research reported in this publication was supported by the National Cancer Institute of the National Institutes of Health under Award Number (R37CA240806). The content is solely the responsibility of the authors and does not necessarily represent the official views of the National Institutes of Health. Approximately, $500k of federal funds supported the effort (50%) on this project. Approximately, $200k of American Cancer Society (133697-RSG-19–110-01-CCE) funds supported a portion of the effort (45%) on this project. The authors would like to acknowledge the support from UCI Chao Family Comprehensive Cancer Center (P30CA062203) (5%).

## DATA AVAILABILITY STATEMENT

The used data can be obtained by contacting the corresponding author.

## REFERENCES

1. Suh Y-G, Noh JM, Lee DY, et al. Proton beam therapy versus photon radiotherapy for stage I non-small cell lung cancer. Cancers. 2022;14(15):3627. doi:10.3390/cancers14153627 [PubMed: 35892885]
2. Kim MM, Verginadis II, Goia D, et al. Comparison of FLASH proton entrance and the Spread-Out Bragg peak dose regions in the sparing of mouse intestinal crypts and in a pancreatic tumor model. Cancers. 2021;13(16):4244. doi:10.3390/cancers13164244 [PubMed: 34439398]
3. Wang X, Pan H, Cheng Q, Wang X, Xu W. Dosimetric deviations of Bragg-peak position shifts in uniform magnetic fields for magnetic resonance Imaging-Guiding proton radiotherapy: a Monte Carlo study. Front Public Health.2021;9:641915.Accessed: Jul. 21, 2023. https://www.frontiersin.org/articles/10.3389/fpubh.2021.641915. [Online]. Available. [PubMed: 34414150]
4. Thasasi P, Ruangchan S, Oonsiri P, Oonsiri S. Determination of integral depth dose in proton pencil beam using plane-parallel ionization chambers. Int J Part Ther. 2022;9(2):1–9. 10.14338/IJPT-22-00006.1
5. Paganetti H, Beltran C, Both S, et al. Roadmap: proton therapy physics and biology. Phys Med Biol. 2021;66(5). doi:10.1088/1361-6560/abcd16
6. Rief H, Chaudhri N, Tonndorf-Martini E, et al. Intensity-modulated radiotherapy versus proton radiotherapy versus carbon ion radiotherapy for spinal bone metastases: a treatment planning study. J Appl Clin Med Phys. 2015;16(6):186–194. doi:10.1120/jacmp.v16i6.5618 [PubMed: 26699573]

7. Kim N, Shin J, Ahn SH, et al. Reduced radiation exposure to circulating blood cells in proton therapy compared with X-ray therapy in locally advanced lung cancer: computational simulation based on circulating blood cells. Front Oncol. 2023;13:1119173. doi:10.3389/fonc.2023.1119173 [PubMed: 36923437]
8. Bayasgalan U, Moon SH, Kim TH, Kim TY, Lee SH, Suh Y-G. Dosimetric comparisons between proton beam therapy and modern photon radiation techniques for stage I non-small cell lung cancer according to tumor location. Cancers. 2021;13(24):6356. doi:10.3390/cancers13246356 [PubMed: 34944976]
9. Hong Z, Yang Z, Mei X. A retrospective study of adjuvant proton radiotherapy for breast cancer after lumpectomy: a comparison of conventional-dose and hypofractionated dose. Radiat Oncol. 2023;18(1):56. doi:10.1186/s13014-023-02213-8 [PubMed: 36959653]
10. Favaudon V, Caplier L, Monceau V. Ultrahigh dose-rate FLASH irradiation increases the differential response between normal and tumor tissue in mice. Sci Transl Med. 2014;6(245):245ra93. doi:10.1126/scitranslmed.3008973
11. Esplen N, Mendonca MS, Bazalova-Carter M. Physics and biology of ultrahigh dose-rate (FLASH) radiotherapy:a topical review. Phys Med Biol. 2020;65(23):23TR03. doi:10.1088/1361-6560/abaa28
12. Diffenderfer ES, Sørensen BS, Mazal A, Carlson DJ. The current status of preclinical proton FLASH radiation and future directions. Med Phys. 2022;49(3):2039–2054. doi:10.1002/mp.15276 [PubMed: 34644403]
13. Vozenin M-C, De Fornel P, Petersson K, et al. The advantage of FLASH radiotherapy confirmed in mini-pig and cat-cancer patients. Clin Cancer Res. 2019;25(1):35–42. doi:10.1158/1078-0432.CCR-17-3375 [PubMed: 29875213]
14. Vozenin M-C, Hendry JH, Limol CL. Biological benefits of ultra-high dose rate FLASH radiotherapy: sleeping beauty awoken. Clin Oncol (R Coll Radiol). 2019;31(7):407–415. doi:10.1016/j.clon.2019.04.001 [PubMed: 31010708]
15. Montay-Gruel P, Petersson K, Jaccard M, et al. Irradiation ina flash: unique sparing of memory in mice after whole brain irradiation with dose rates above 100 Gy/s. Radiother Oncol. 2017;124(3):365–369. doi:10.1016/j.radonc.2017.05.003 [PubMed: 28545957]
16. Schüler E, Acharya M, Montay-Gruel P, Loo BW Jr, Vozenin M-C, Maxim PG. Ultra-high dose rate electron beams and the FLASH effect: from preclinical evidence to a new radiotherapy paradigm. Med Phys. 2022;49(3):2082–2095. doi:10.1002/mp.15442 [PubMed: 34997969]
17. Bogaerts E, Macaeva E, Isebaert S, Haustermans K. Potential molecular mechanisms behind the ultra-high dose rate 'FLASH' effect. Int J Mol Sci. 2022;23(20):12109. doi:10.3390/ijms232012109 [PubMed: 36292961]
18. Darafsheh A, Hao Y, Zwart T, et al. Feasibility of proton FLASH irradiation using a synchrocyclotron for preclinical studies. Med Phys. 2020;47(9):4348–4355. doi:10.1002/mp.14253 [PubMed: 32452558]
19. Wei S, Shi C, Chen CC, et al. Recent progress in pencil beam scanning FLASH proton therapy: a narrative review. Ther Radiol Oncol. 2022;6(0):16. 10.21037/tro-22-1
20. Zarifi M, Qi Y, Guatelli S, Hutton B, Rosenfeld A, Investigation of optimized prompt gamma detection strategy for real-time Bragg peak tracking in proton radiation therapy. In: 2015 IEEE Nuclear Science Symposium and Medical Imaging Conference (NSS/MIC). IEEE; 2015;1–5. doi:10.1109/NSSMIC.2015.7582237
21. Lourenço A, Subiel A, Lee N, et al. Absolute dosimetry for FLASH proton pencil beam scanning radiotherapy. Sci Rep. 2023;13(1):2054. doi:10.1038/s41598-023-28192-0 [PubMed: 36739297]
22. Romano F, Bailat C, Jorge PG, Lerch MLF, Darafsheh A. Ultra-high dose rate dosimetry: challenges and opportunities for FLASH radiation therapy. Med Phys. 2022;49(7):4912–4932. doi:10.1002/mp.15649 [PubMed: 35404484]
23. Zhang Q, Cascio E, Li C, et al. FLASH investigations using protons: design of delivery system, preclinical setup and confirmation of FLASH effect with protons in animal systems. Radiat Res. 2020;194(6):656–664. doi:10.1667/RADE-20-00068.1 [PubMed: 32991708]

24. Konradsson E, Ceberg C, Lempart M, et al. Correction for ion recombination in a built-in monitor chamber of a clinical linear accelerator at ultra-high dose rates. Radiat Res. 2020;194(6):580–586. doi:10.1667/RADE-19-00012 [PubMed: 33348371]
25. Cavallone M, Gonçalves Jorge P, Moeckli R, et al. Determination of the ion collection efficiency of the Razor Nano Chamber for ultra-high dose-rate electron beams. Med Phys.2022;49(7):4731–4742. doi:10.1002/mp.15675 [PubMed: 35441716]
26. Hickling S, Xiang L, Jones KC, et al. Ionizing radiation-induced acoustics for radiotherapy and diagnostic radiology applications. Med Phys. 2018;45(7):e707–e721. doi:10.1002/mp.12929 [PubMed: 29679491]
27. Jiang Z, Sun L, Yao W, Wu QJ, Xiang L, Ren L. 3D in vivo dose verification in prostate proton therapy with deep learning-based proton-acoustic imaging. Phys Med Biol. 2022;67(21):215012. doi:10.1088/1361-6560/ac9881
28. Jones KC, Witztum A, Sehgal CM, Avery S. Proton beam characterization by proton-induced acoustic emission: simulation studies. Phys Med Biol. 2014;59(21):6549–6563. doi:10.1088/0031-9155/59/21/6549 [PubMed: 25322212]
29. Gonzalez G, Prather K, Pandey PK, et al. Single-Pulse X-ray acoustic computed tomographic imaging for precision radiation therapy. Adv Radiat Oncol. 2023;8(4):101239. doi:10.1016/j.adro.2023.101239 [PubMed: 37334315]
30. Kellnberger S, Assmann W, Lehrack S, et al. Ionoacoustic tomography of the proton Bragg peak in combination with ultrasound and optoacoustic imaging.Sci Rep.2016;6(1):29305.doi:10.1038/srep29305 [PubMed: 27384505]
31. Præsius SK, Stuart MB, Schou M, Dammann B, Brandenborg Sørensen HH, Jensen JA, Real-time super-resolution ultrasound imaging using GPU acceleration. In: 2022 IEEE International Ultrasonics Symposium (IUS). IEEE; 2022;1–4. doi:10.1109/IUS54386.2022.9957589
32. Takayanagi T, Uesaka T, Nakamura Y, et al. On-line range verification for proton beam therapy using spherical ionoacoustic waves with resonant frequency. Sci Rep. 2020;10(1):20385. doi:10.1038/s41598-020-77422-2 [PubMed: 33230208]
33. Sueyasu S, Takayanagi T, Miyazaki K, et al. Ionoacoustic application of an optical hydrophone to detect proton beam range in water. Med Phys. 2023;50(4):2438–2449. doi:10.1002/mp.16189 [PubMed: 36565440]
34. Sulak L, Armstrong T, Baranger H, et al. Experimental studies of the acoustic signature of proton beams traversing fluid media. Nucl Instrum Methods. 1979;161(2):203–217. doi:10.1016/0029-554X(79)90386-0
35. Xia J, Yao J, Wang LV. Photoacoustic tomography: principles and advances. Electromagn Waves. 2014;147:1–22.
36. Hysi E, Moore MJ, Strohm EM, Kolios MC. A tutorial in photoacoustic microscopy and tomography signal processing methods. J Appl Phys. 2021;129(14):141102. doi:10.1063/5.0040783
37. Xu M, Wang LV. Universal back-projection algorithm for photoacoustic computed tomography. Phys Rev E Stat Nonlin Soft Matter Phys. 2005;71(1):016706. doi:10.1103/PhysRevE.71.016706 [PubMed: 15697763]
38. Hickling S, Hobson M, Naqa IE. Characterization of X-ray acoustic computed tomography for applications in radiotherapy dosimetry. IEEE Trans Radiat Plasma Med Sci. 2018;2(4):337–344. doi:10.1109/TRPMS.2018.2801724
39. Ahmad M, Xiang L, Yousefi S, Xing L. Theoretical detection threshold of the proton-acoustic range verification technique. Med Phys. 2015;42(10):5735–5744. doi:10.1118/1.4929939 [PubMed: 26429247]
40. Oraiqat I, Zhang W, Litzenberg D, et al. An ionizing radiation acoustic imaging (iRAI) technique for real-time dosimetric measurements for FLASH radiotherapy. Med Phys.2020;47(10):5090–5101. doi:10.1002/mp.14358 [PubMed: 32592212]
41. Gerlach S, Balling F, Schmidt AK, et al. Three-dimensional acoustic monitoring of laser-accelerated protons in the focus of a pulsed-power solenoid lens. High Power Laser Sci Eng. 2023;11:e38. doi:10.1017/hpl.2023.16

42. Bergen R, Sun L, Pandey PK, et al. Discrete wavelet transformation for the sensitive detection of ultrashort radiation pulse with radiation-induced acoustics. IEEE Trans Radiat Plasma Med Sci. 2024;8:76–87. [PubMed: 39220226]
43. Darafsheh A, Hao Y, Zhao X, et al. Spread-out Bragg peak proton FLASH irradiation using a clinical synchrocyclotron: proof of concept and ion chamber characterization. Med Phys. 2021;48(8):4472–4484. doi:10.1002/mp.15021 [PubMed: 34077590]
44. Caron J, Gonzalez G, Pandey PK, et al. Single pulse protoacoustic range verification using a clinical synchrocyclotron. Phys Med Biol. 2023;68(4):045011. doi:10.1088/1361-6560/acb2ae
45. Patch SK, Kireeff Covo M,Jackson A, et al. Thermoacoustic range verification using a clinical ultrasound array provides perfectly co-registered overlay of the Bragg peak onto an ultrasound image. Phys Med Biol. 2016;61(15):5621–5638. doi:10.1088/0031-9155/61/15/5621 [PubMed: 27385261]
46. Kim K, Pandey PK, Gonzalez G, Chen Y, Xiang L. Simulation study of protoacoustics as a real-time in-line dosimetry tool for FLASH proton therapy. Med Phys. 2024;51:5070–5080. doi:10.1002/mp.16894 [PubMed: 38116792]
47. Pandey PK, Wang S, Aggrawal HO, Bjegovic K, Boucher S, XiangL. Model-based X-ray-induced acoustic computed tomography. IEEE Trans Ultrason Ferroelectr Freq Control. 2021;68(12):3560–3569. doi:10.1109/TUFFC.2021.3098501 [PubMed: 34310297]
48. Pandey PK, Wang S, Sun L, Xing L, Xiang L. Model-based 3-D X-ray induced acoustic computerized tomography. IEEE Trans Radiat Plasma Med Sci.2023;7(5):532–543.doi:10.1109/TRPMS.2023.3238017 [PubMed: 38046375]
49. Jiang Z, Wang S, Xu Y, et al. Radiation-induced acoustic signal denoising using a supervised deep learning framework for imaging and therapy monitoring. Phys Med Biol. 2023;68(23):235010. doi:10.1088/1361-6560/ad0283
50. Lang Y, Jiang Z, Sun L, Xiang L, Ren L. Hybrid-supervised deep learning for domain transfer 3D protoacoustic image reconstruction. ArXiv. 2023. arXiv:2308.06194v1.

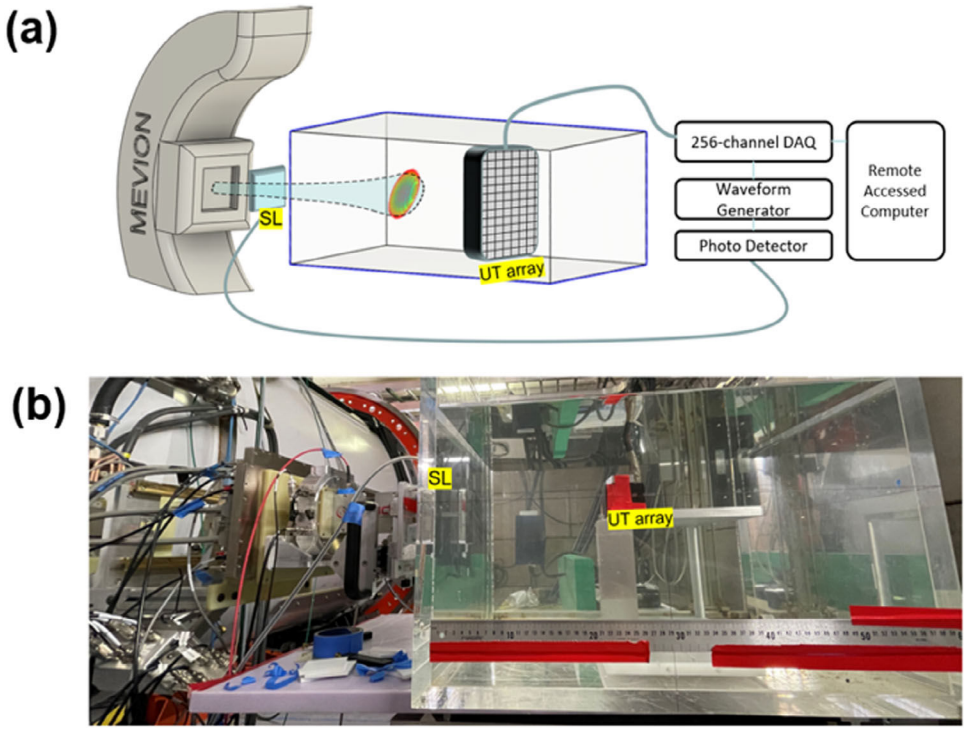


**FIGURE 1.**

Protoacoustic measurement setup. (a) schematic view of the experimental setup (b) Mevion prototype FLASH source setup. SL: scintillator for trigger purposes. UT array: 256-element planar ultrasound transducer array. FLASH, Fast low angle shot hyperfractionation.

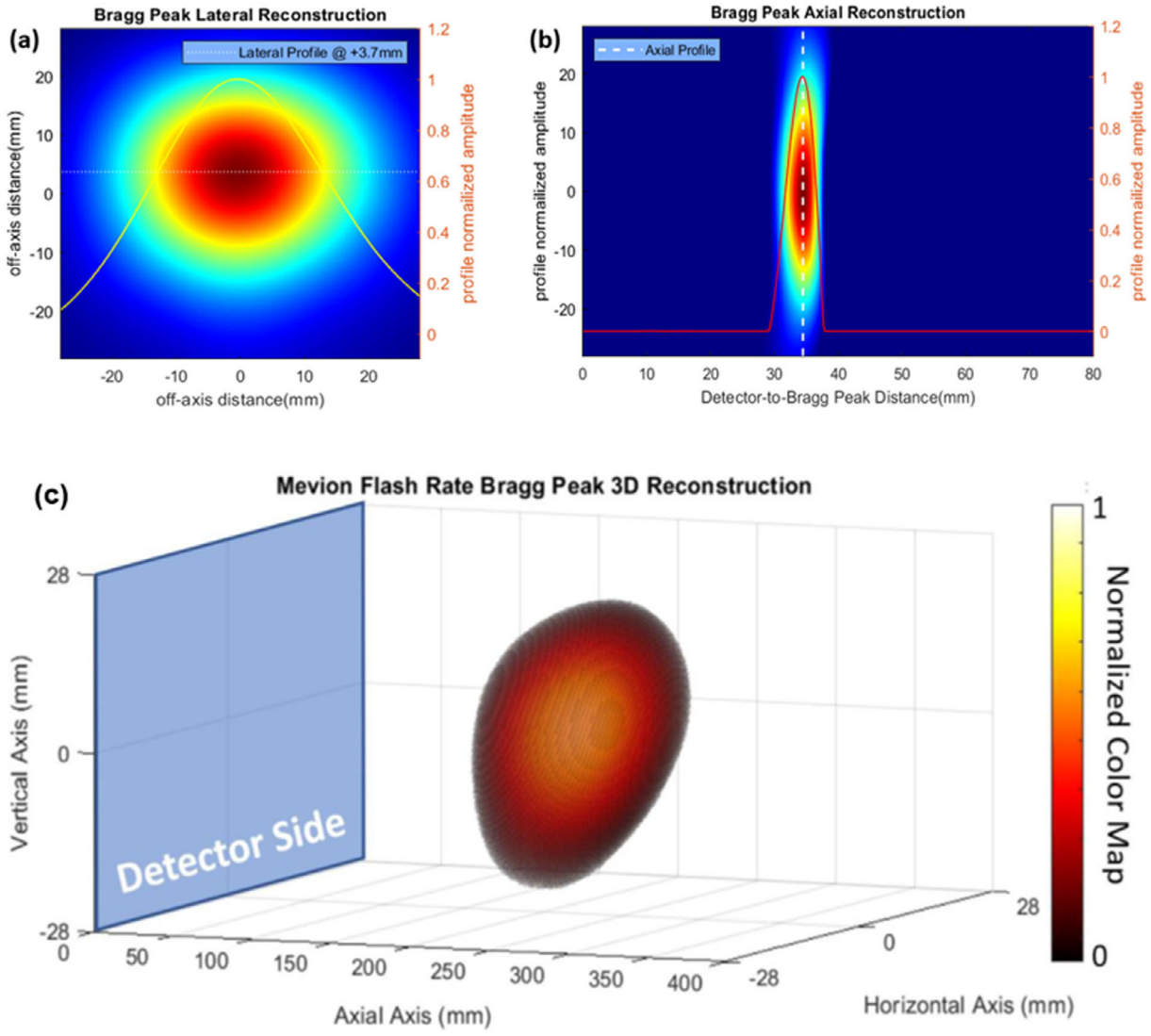


**FIGURE 2.**

3D Protoacoustic imaging of Bragg peak. (a) Protoacoustic imaging demonstrates a lateral reconstruction slice at the Bragg peak center of a FLASH rate proton beam, utilizing a 256-element planar ultrasound transducer array. The dashed white line marks the location from which the Bragg peak's lateral profile is extracted, depicted by the solid yellow line. (b) Protoacoustic imaging illustrates an axial reconstruction slice at the center of the Bragg peak for a FLASH rate proton beam. Here, the dashed white line shows the point of extraction for the Bragg peak's axial profile, represented by the solid red line. (c) Protoacoustic imaging reveals the 3D volumetric dose distribution for a FLASH rate proton beam. 3D, three-dimensional; FLASH, Fast low angle shot hyperfractionation.

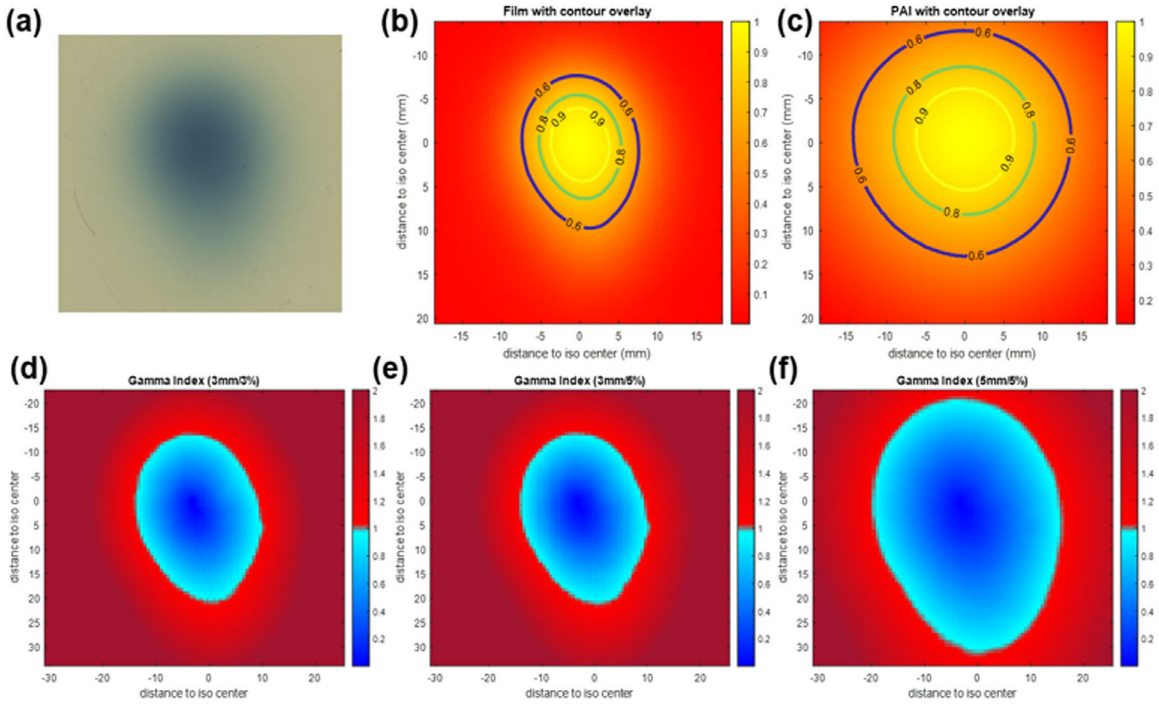


**FIGURE 3.**

PAI versus film using gamma index analysis. (a) picture of the film result of a single proton pulse. (b) extracted normalized film value. (c) PAI reconstructed the slice at the Bragg peak. (d)–(f) Gamma index analysis. Points with a $\gamma$-index value less than 1 pass the test (in blue shades). PAI, proton-induced acoustic imaging.

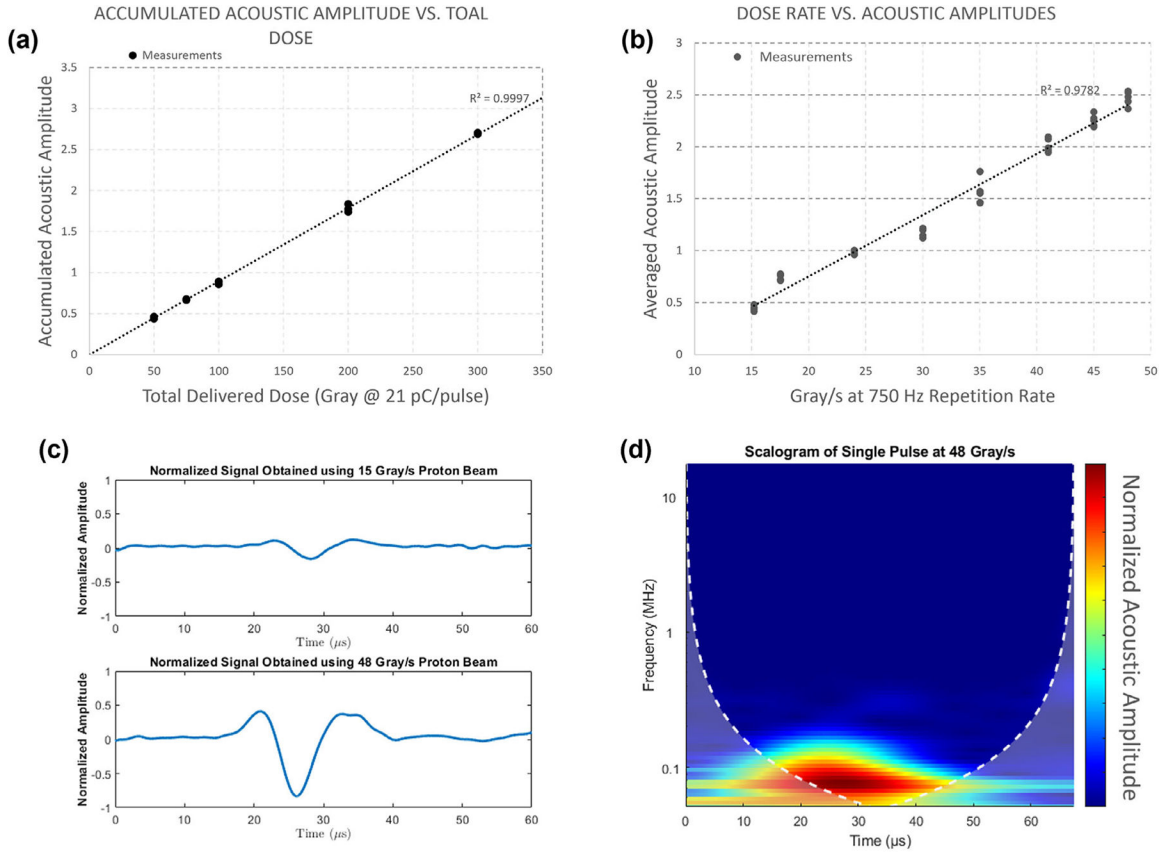


**FIGURE 4.**

Dose Linearity Study in FLASH regime with PA measurement. (a) Verified accumulated dose delivered (at 50, 150, 100, 200, and 300 Gy) versus protoacoustic amplitude measurements. Each total dose level was repeated three times. The acoustic signal amplitude is extracted from the center channel of the planar array. (b) Verified dose rate delivered (at 15.2, 17.5, 24, 30, 45, and 48 Gy/s) versus protoacoustic amplitude measurements. (c) Direct comparison of averaged protonacoustic signals obtained from 15 and 48 Gy/s, respectively. (d) The scalogram of a single pulse obtained at 48 Gy/s proton beam, demonstrates the typical frequency components of obtained signals. FLASH, Fast low angle shot hyperfractionation.

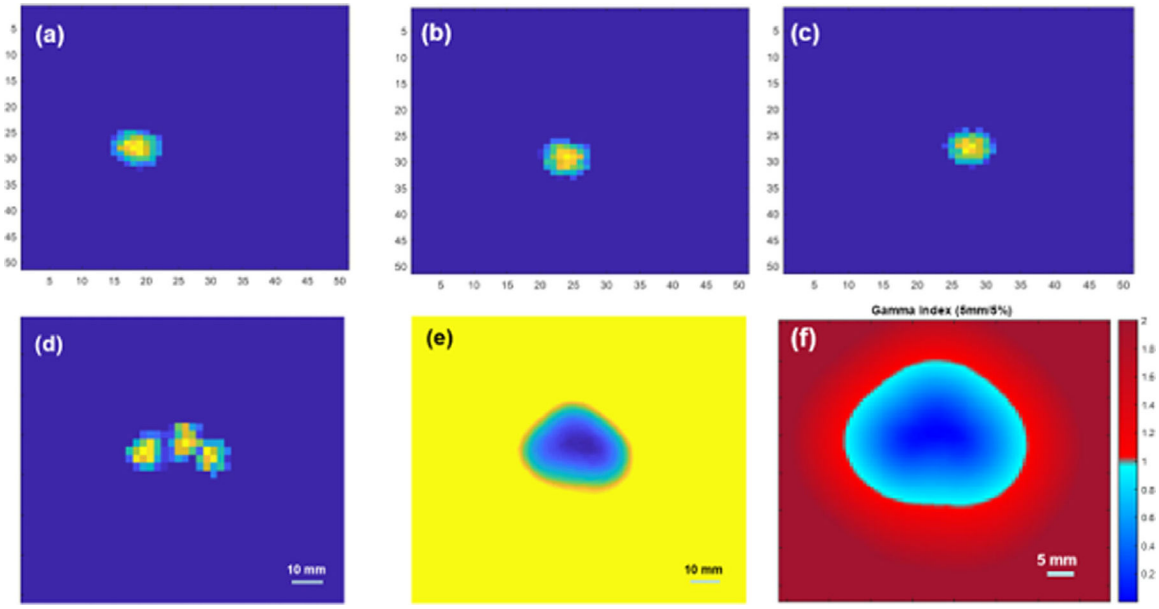


**FIGURE 5.**

FLASH proton beams 3-dot scan tracking using PAI. (a)–(c) scanning locations of each Bragg peaks. (d) superimposed 3-dot scanning pattern PAI reconstruction. (e) 3-dot pattern verification using film. (f) 3-dot pattern gamma index mapping for superimposed PAI imaging result and the film result using 5 mm/5% criteria. FLASH, Fast low angle shot hyperfractionation; PAI, proton-induced acoustic imaging.

**TABLE 1**

Experimental parameters.

| Experiment | Depth of transducter (cm) | Ion source pulse width (us) | FLASH TIC recycling (nC) | Estimated average charge per pulse (pC/pulse) | Estimated average dose rate [total dose/total time] (Gy/s) | Estimated dose per pulse (Gy/pulse) |
|---|---|---|---|---|---|---|
| Dose rate/PA amplitude comparison | 25.6 | 8 | 33.06 | 3.31 | 15.21 | 0.020 |
| Dose rate/PA amplitude comparison | 25.6 | 10 | 39.63 | 7.93 | 18.24 | 0.048 |
| Dose rate/PA amplitude comparison | 25.6 | 10.7 | 21.90 | 10.95 | 25.19 | 0.067 |
| Dose rate/PA amplitude comparison | 25.6 | 12.7 | 89.44 | 17.89 | 41.15 | 0.109 |
| All other experiments | 25.6 | 14 | 104.06 | 20.81 | 47.88 | 0.127 |

**TABLE 2**

Gamma index analysis.

| Type | Gamma Index | 10% low-dose threshold | 30% low-dose threshold | 50% low-dose threshold |
|---|---|---|---|---|
| Single | 3 mm/3% | 33.06% | 59.13% | 89.40% |
| Single | 3 mm/5% | 34.21% | 61.17% | 91.43% |
| Single | 5 mm/5% | 76.40% | 100.00% | 100.00% |
| 3-dot | 5 mm/5% | 40.13% | 70.67% | 82.88% |